Journal of Renewable Materials

Tech Science Press

DOI: 10.32604/jrm.2024.054047

ARTICLE

Enhanced Dye Adsorption and Bacterial Removal of Magnetic Nanoparticle-Functionalized Bacterial Cellulose Acetate Membranes

Heru Suryanto[1,2,*], Daimon Syukri[3], Fredy Kurniawan[4], Uun Yanuhar[5], Joseph Selvi Binoj[6], Sahrul Efendi[2], Fajar Nusantara[2], Jibril Maulana[7], Nico Rahman Caesar[5] and Komarudin Komarudin[2]

[1]Centre of Advanced Material for Renewable Energy (CAMRY), Universitas Negeri Malang, Malang, 65145, Indonesia

[2]Department of Mechanical and Industrial Engineering, Universitas Negeri Malang, Malang, 65145, Indonesia

[3]Department of Food and Agricultural Product Technology, Faculty of Agricultural Technology, Andalas University, Padang, 25163, Indonesia

[4]Department of Chemistry, Institut Teknologi Sepuluh Nopember, Surabaya, 60111, Indonesia

[5]Study Program of Aquatic Resources Management, Faculty of Fisheries and Marine Science, Brawijaya University, Malang, 65145, Indonesia

[6]Institute of Mechanical Engineering, Saveetha School of Engineering, Saveetha Institute of Medical and Technical Sciences (SIMATS), Saveetha University, Chennai, 602105, India

[7]Faculty of Vocational, Universitas Negeri Malang, Malang, 65145, Indonesia

[*]Corresponding Author: Heru Suryanto. Email: heru.suryanto.ft@um.ac.id

Received: 17 May 2024 Accepted: 02 August 2024 Published: 25 September 2024

ABSTRACT

Utilizing biomass waste as a potential resource for cellulose production holds promise in mitigating environmental consequences. The current study aims to utilize pineapple biowaste extract in producing bacterial cellulose acetate-based membranes with magnetic nanoparticles (Fe_3O_4 nanoparticles) through the fermentation and esterification process and explore its characteristics. The bacterial cellulose fibrillation used a high-pressure homogenization procedure, and membranes were developed incorporating 0.25, 0.50, 0.75, and 1.0 wt.% of Fe_3O_4 nanoparticles as magnetic nanoparticle for functionalization. The membrane characteristics were measured in terms of Scanning Electron Microscope, X-ray diffraction, Fourier Transform Infrared, Vibrating Sample Magnetometer, antibacterial activity, bacterial adhesion and dye adsorption studies. The results indicated that the surface morphology of membrane changes where the bacterial cellulose acetate surface looks rougher. The crystallinity index of membrane increased from 54.34% to 68.33%, and the functional groups analysis revealed that multiple peak shifts indicated alterations in membrane functional groups. Moreover, adding Fe_3O_4-NPs into membrane exhibits paramagnetic behavior, increases tensile strength to 73%, enhances activity against *E. coli* and *S. aureus*, and is successful in removing bacteria from wastewater of the river to 67.4% and increases adsorption for anionic dyes like Congo Red and Acid Orange.

KEYWORDS

Bacterial cellulose; dye adsorption; Fe_3O_4 nanoparticles; membrane; pineapple; waste

Nomenclature

AO	Acid Orang
BC	Bacterial Cellulose
BCA	Bacterial Cellulose Acetate
CA	Cellulose Acetate
CH_3COOH	Acetic Acid
CrI	Crystallinity Index
CR	Congo Red
dH_2O	Distilled Water
Fe_3O_4	Iron Oxide
FTIR	Fourier Transform Infrared
FWHM	Full Width at Half-Maximum
Hc	Coercivity Value
L	Crystallite Size
MB	Methylene Blue
Mr	Remanence
Ms	Magnetization Saturation
NPs	Nanoparticle
Rh	Rhodamin
ROS	Reactive Oxygen Species
SEM	Scanning Electron Microscope
VSM	Vibrating Sample Magnetometer
XRD	X-Ray Diffraction

1 Introduction

Lignocellulose, a biopolymer widely distributed on earth, is produced in significant quantities annually, estimated at approximately 181.5 billion tons globally [1]. The total trade value in 2022 reached $7.5 billion [2]. This natural polymer comprises large molecules composed of β-D-glucopyranose units connected by β(1,4)-glycosidic bonds [3]. Cellulose demand has contributed to deforestation, posing environmental challenges. Using biomass waste for cellulose production provides an alternative strategy to reduce environmental impact, offering significant benefits.

In 2020, Indonesia's pineapple fruit production reached approximately 2.5 million tons, among the world's top ten pineapple-exporting nations [4]. Processing pineapple fruit can leave about 10% of pineapple peel biowaste [5], generating about 250,000 tons per year of pineapple peel biowaste in Indonesia. This biowaste can serve as a fermentation medium to produce cellulose from bacteria. Bacteria produce cellulose by synthesizing a biopolymer consisting of (1→4)-β-glucan chains, forming microfibrils that assemble into ribbon-like structures, ultimately creating 3D networks known as pellicles [6]. Similar to cellulose, these structures share the general formula $(C_6H_{10}O_5)n$. Bacterial cellulose (BC) has a degree of substitution that varies from 0.04 to 2.77 depending on the concentration of acetic anhydride when it converts to cellulose acetate (CA) [7]. Developing membranes from such biopolymers is particularly intriguing due to their versatile applications, spanning from purification membranes [8], catalysts [9], fuel cells [10], and even wound dressings [11]. The potency of these membranes can be further enhanced by incorporating nanomaterials within them for better performance.

CA, a cellulose derivative, can be easily obtained from natural resources and recycled into the environment by the biodegradation process. Their membrane offers flexibility for integrating with nanoparticles, superior transport characteristics, higher mechanical strength, higher hydrophilicity, and excellent film-forming properties during the membrane fabrication process [12]. Nonetheless, enhancements are required in terms of permeability, strength, thermal stability, vulnerability to fouling, and salt rejection for CA membranes to rival thin-film nanocomposites effectively [13]. Incorporating nanomaterials into composites can alter composite's attributes, introducing distinct supplementary functionalities. Nanoparticles (NPs) provide a method for customizing CA membranes. Various nanomaterials, including carbon nanotubes [14], titania [15], silicate [16], zinc oxide [17], graphite nanoplatelets [18], and graphene [19], have been introduced into polymer membranes to enhance their characteristics.

Magnetic nanoparticles are a category of nanoparticles that can be controlled through the application of magnetic fields. They have garnered significant attention due to their utilization in specific domains like catalysis, biomedical, biosensing, and environmental applications. Furthermore, incorporating magnetic nanoparticles has emerged as another avenue for enhancing membrane performance. Magnetic materials such as Fe_3O_4 nanoparticles (Fe_3O_4-NPs) have hydrophilic properties [20]. So, it facilitates the creation of intermolecular bonds between the oxygen in Fe_3O_4 nanoparticles and hydroxyl groups, which are facilitated by surplus electrons furnished by hydroxyl groups [21]. Another form of intermolecular bonding emerges from the electrostatic force between the surface of Fe_3O_4-NPs and cellulose fibril. The electrostatic force of Fe_3O_4-NPs is beneficial for dye adsorption [22]. Moreover, the mechanical interlocking causes Fe_3O_4-NPs to inhibit the movement of fibrils, consequently bolstering the strength of nanocomposite [23,24]. Fe_3O_4-NPs systems have effectively killed bacteria and destructed biofilms [25]. So, this study aims to explore the use of pineapple biowaste extract to produce bacterial cellulose acetate (BCA) membranes functionalized with Fe_3O_4-NPs by *ex-situ* methods and reveal their characteristics so that they can provide benefits for environmental sustainability. The characteristic of the membranes was confirmed by X-Ray Diffraction (XRD), Scanning Electron Microscope (SEM), Fourier Transform Infrared (FTIR), Vibrating Sample Magnetometer (VSM), agar disk diffusion methods, dye adsorption, and bacteria adhesion test.

2 Experimental

2.1 Materials

Pineapple peel biowaste was collected from a plantation in the Blitar region, East Java, Indonesia. *Acetobacter xylinum* was obtained from the Applied Tech-Laboratory at Universitas Muhamadiyah, Malang, Indonesia, and used as cellulose producer bacteria. Chemical substances used in the BC production were NaOH (purity 32%, Smart-Lab, Jakarta, Indonesia), urea (purity 99.5%, Smart-Lab, Jakarta, Indonesia), acetic acid (purity 99.7%, Smart-Lab, Jakarta, Indonesia), glucose (purity 99%, Smart-Lab, Jakarta, Indonesia), and ammonia (purity 99.8%, Smart-Lab, Jakarta, Indonesia). Fe_3O_4-NPs with particle sizes of 30–50 nm (purity 99.8%, Guangzhou Hongwu Co., Guangzhou, Guangdong, China) were utilized to increase the functionalization of the membrane.

2.2 Bacterial Cellulose Production

The fabrication of BC followed established protocols outlined in prior publications [26]. The medium for fermentation was formulated using a mixture of 1.0 L extract of pineapple peel biowaste, 5.0 g ammonia, and 100.0 g glucose. The medium was controlled at pH-4.5 by adding CH_3COOH solution. The fermentation process involved introducing 100 mL of *Acetobacter xylinum* to the medium, and static fermentation was carried out at 25°C–30°C. Subsequently, BC pellicle floated on media, and within 10 days, BC was collected and washed with distilled water (dH_2O) to achieve pH-7.0.

2.3 Bacterial Cellulose Fibrillation

The fibrillation of BC was done according to a previous study [27]. The pellicles were pre-treated using immersion in 6% NaOH solution for 2 h at 90°C. The treated pellicles were rinsed and subsequently cut into smaller segments. 300 g of these cleaned pellicles was soaked in 250 mL dH_2O and processed in a crusher (Fomac, Jakarta, Indonesia) at 26,000 rpm for 5 min. The resulting BC slurry was mixed with 750 mL of distilled water and subsequently subjected to a High-Pressure Homogenizer (Berkley Sci., AH100D, Shanghai, China). Fibrillation of BC was carried out under a pressure of 150 bar, followed by a filtering process to collect BC slurry.

2.4 BCA Synthesis

Synthesis of BCA followed previously published methods [28]. BNC 2.50 g was placed in a beaker glass and filled with 50 mL of glacial acetic acid. The mixture was stirred for a duration of 30 min. To this solution, 0.32 mL of H_2SO_4 (purity 97%–97%, Smart-Lab, Indonesia) and 18 mL of CH_3COOH solution (purity 99.9%, Smart-Lab, Indonesia) were introduced, and stirring continued for 25 min. Afterward, the solution underwent filtration followed by 64 mL of anhydrous acetate, incorporated into the filtrate and stirred for 30 min. The solution was set aside for 14 h and filtered under a vacuum. The ensuing precipitates were washed with dH_2O until neutral and subsequently dried for 12 h at 70°C in an oven (Kirin, Indonesia).

2.5 Synthesis of BCA/Fe_3O_4-NPs Membrane

The preparation of cellulose acetate was conducted in accordance with established protocols [29]. Wet BCA filtrate (obtained from Section 2.4) was suspended in 200 mL dH_2O, stirred for 30 min, and subjected to sonication for 30 min at 400 watts, 20,000 Hz (Lawson Scientific, UP.400S-type, Zhejiang, China). During this process, Fe_3O_4-NPs were introduced to the dispersion and subjected to sonication for 30 min. As mentioned, the dispersion was continually stirred for 2 h to attain a uniform suspension, and the mixture was then placed in an oven at 120°C for 4 h. Afterward, cellulose acetate was mixed into the homogeneous mixture and homogenized for 1 h using ultrasonication. Finally, the solution was cast into a mold and dried in an oven at 60°C for 24 h.

2.6 Crystallinity Analysis

The XRD test assessed the crystallinity of BCA/Fe_3O_4-NPs nanocomposite membrane using a Panalytical-Expert Pro instrument from the USA. For XRD testing, samples sized 20 mm^2 × 20 mm^2 were prepared. Scanning was conducted from 5° to 75° diffraction using a CuKα at λ of 1.542Å, 30.0 mA and 40.0 kV. Crystallite size (L) was calculated by Eq. (1), while the crystallinity index (CrI) was calculated using Eq. (2) [30]:

$$L = \frac{K\lambda}{\beta \cos\theta} \tag{1}$$

where K was Scherrer's constant (0.89); λ was the wavelength of the X-ray; θ was the diffraction angle; β was full width at half-maximum (FWHM) (rad).

$$CrI = \frac{I_{22} - I_{18}}{I_{22}} \times 100\% \tag{2}$$

where I_{22} was the peak intensity at 2θ of about 22.0°. I_{18} was the lowest intensity of 2θ at about 18°.

XRD data was analyzed using Origin 9 software and Match software v.3.16.

2.7 FTIR Analysis

FTIR analysis was conducted on an Infrared instrument (Prestige-21, Shimadzu, Japan). The membrane was dried at 105°C for 3 h in an oven, then grinded to get a powdered sample. 1.0 mg of KBr powder was mixed with membrane powder of 0.1 mg and subsequently compressed to form a solid pellet. FTIR scanning analysis was conducted in wavenumber 400 to 4000 cm^{-1} with a scanning rate of 2 cm^{-1}.

2.8 Morphology Observation

The SEM (Inspect S50, FEI, Hillsboro, OR, USA) examined the surface morphology at an acceleration voltage of 25.0 kV. Prior to SEM observation, membrane samples were coated using a gold layer until a thickness of 10 nm using a coater (Emitech, SC7.620, Chelmsford, UK).

2.9 Magnetic Properties Analysis

The magnetic properties of nanocomposite of BCA/Fe_3O_4-NPs were analyzed using VSM (Oxford Instrument, type 1.2H, Abingdon, UK) with a magnetic field up to an applied magnetic field between −30 kOe and 30 kOe at room temperature with a nanocomposite weight of at least 50 mg.

2.10 Antibacterial Test

The antimicrobial activity of the membrane was evaluated using agar disk diffusion techniques [31] with both gram-negative bacteria (*Escherichia coli*) and gram-positive bacteria (*Staphylococcus aureus*) (Microbiology lab. UM, Malang, Indonesia). The membrane was cut into small pieces with a diameter of 5 mm. To ensure sterility and remove any acidic content, the samples were heated and subjected to overnight ultraviolet light exposure. The plates were filled with an agar medium of Muller-Hinton (Oxoid, Basingstoke, UK), and spread the bacteria along the surface by applying bacterial loops. Following the inoculation of plates, the membrane sample was placed on them and incubated at 36°C for 24 h.

2.11 Dye Removal Analysis

BCA/Fe_3O_4-NPs membrane sample was cut into ±2 cm^2. Membranes were then immersed in AZO solutions like Congo Red (CR), Methylene Blue (MB), Rhodamine (Rh), and Acid Orange (AO) with a concentration of 10 ppm in tube 50 mL. Membranes in Azo solution were left in a tube for 5 h. The membrane was taken using a tweezer; then, Azo solution was tested by UV-visual spectrophotometer (Thermo Scientific, Waltham, MA, USA) with the wavelengths for CR, MB, Rh, and AO of 470, 685, 553, and 479 nm, respectively. The adsorption of AZO dyes was then calculated to obtain the percentage of dye adsorption.

2.12 Bacteria Adhesion Test

Wastewater samples were obtained from two rivers in Padang Town (West Sumatera, Indonesia) contaminated with factory waste, which was still used by local communities, by setting the collection location 200–300 m from the drain. Before the adhesion test was carried out, supporting devices such as reaction tubes, and pipette tips were cleaned and wet sterilized using an autoclave at 121°C for 2 h. For clean, dry sterilization was carried out using an oven for 2 h at 180°C. Salt (NaCl 0.9%) as a dilution medium was wet sterilized by putting 9 mL into a test tube, then the test tube was closed using a layer of cotton and aluminum foil. The finished media was then wet sterilized using an autoclave at 121°C for 2 h. The water sample was shaken and placed in a 10 mL sterile test tube. The membrane was cut to a diameter of 20 mm and put into a test tube containing wastewater samples by clamping it using sterile tweezers for 10 min. The membrane was removed and stored for testing and then incubated in a test tube at 25°C for a day. The growth media used to observe microbial growth are Plate Count Agar and Luria

Agar media. Then, the microbes that adhere to the filter are washed and diluted for subsequent enumeration using the pour plate technique [32].

2.13 Tensile Test

A tensile strength test of the BCA membrane was performed by a tensile tester (Techno-Lab, Malang, Indonesia), which had a maximum load of 50 N. The membranes were cut with dimensions following ASTM D638-V. The specimens were clamped in the holders, and five specimens for each treatment were pulled at 3 mm/min. Statistical analysis was conducted using one-way ANOVA methods using Origin software v.9.0, continuing with Tukey analysis.

3 Results and Discussions

3.1 Morphology Analysis

Preparation of BCA nanocomposite through homogenization and cast methods results in membranes with a thickness of 23 ± 1.5 μm. The membrane was observed under SEM, and the morphology of Fe_3O_4-NPs to BCA membrane is depicted in Fig. 1. It shows a smooth morphology with small pores (Fig. 1A). With the addition of Fe_3O_4-NPs 0.25 wt.%, the surface of BCA membrane is rough (Fig. 1B). Several Fe_3O_4-NPs appeared on the surface. Fe_3O_4-NPs content of 0.50 wt.% appears to a little agglomeration of Fe_3O_4-NPs, causing the surface to rougher (Fig. 1C) due to Fe_3O_4-NPs tend to adhere and subsequently agglomeration, which is characteristics of their nature [33].

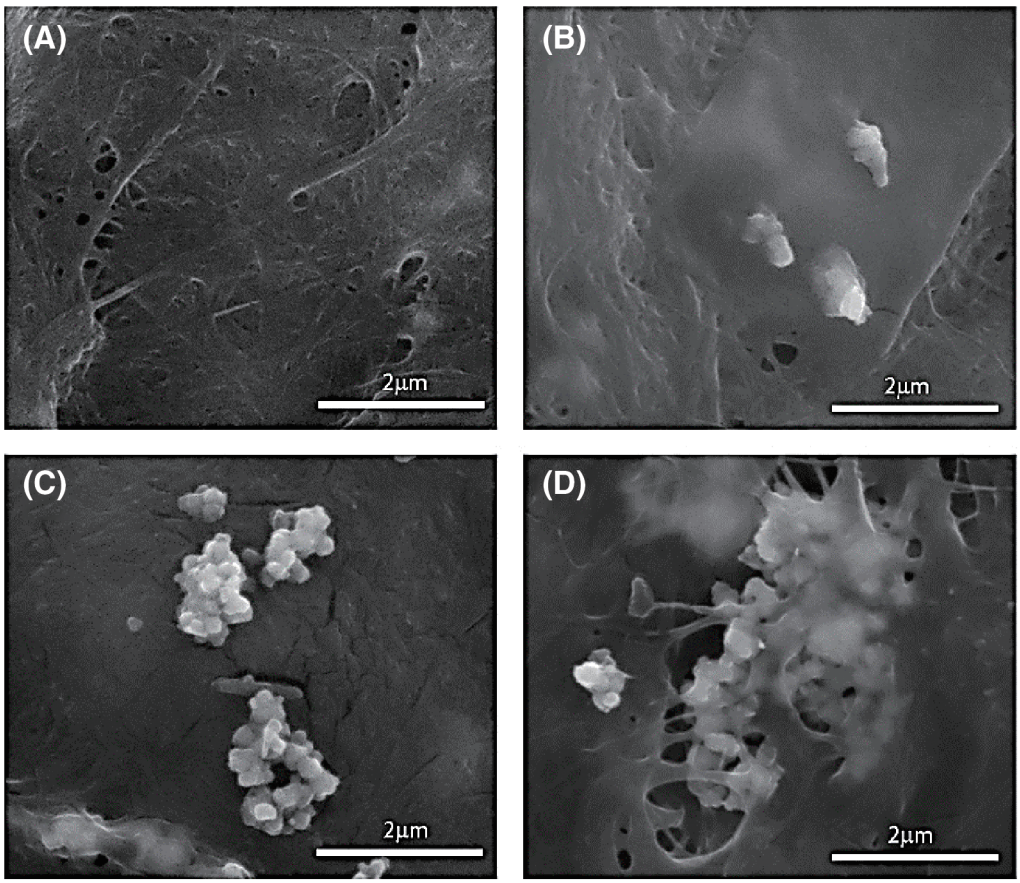

Figure 1: (Continued)

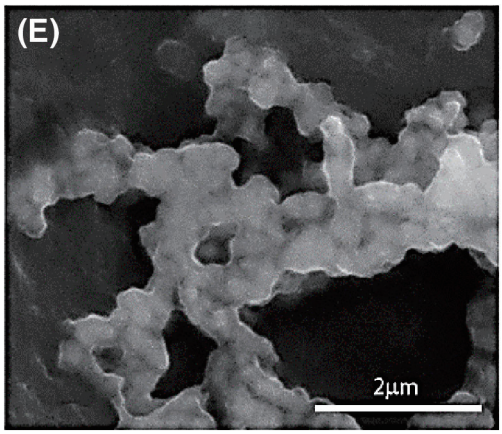

Figure 1: Surface morphology of membrane BCA with (A) control (without Fe_3O_4-NPs), (B) Fe_3O_4-NPs 0.25 wt.%, (C) Fe_3O_4-NPs 0.50 wt.%, (D) Fe_3O_4-NPs 0.75 wt.%, and (E) Fe_3O_4-NPs 1.00 wt.%

The introduction of 0.75 and 1.0 wt.% of Fe_3O_4-NPs leads to an agglomeration on the pore of the BCA nanocomposite membrane (Fig. 1D,E). Besides Fe_3O_4-NPs appearing on the surface, they also intruded into the internal network of BCA membrane, and bigger agglomerates were found in the membrane. The interaction of Fe_3O_4-NPs with cellulose via hydrogen bonding between the hydroxyl groups on the surfaces of both particles [21] implies membrane morphology. A higher content of Fe_3O_4-NPs attracts more nanofiber, so it clumps together and produces more pores in the membrane.

3.2 Membrane Structure Analysis

Fig. 2 depicts the diffractogram of BCA/Fe_3O_4-NPs membrane, which contains 3 main peaks at 14.17°, 16.59°, and 22.46° corresponding to crystal plane [100], [010], and [110], respectively. The d-spacings at peaks about 14° and 16° show the value in the range of 0.615–0.624 nm and 0.527–0.543 nm (Table 1), respectively. This structure is indicated as Iα rich-type cellulose [34]. Nanocomposite membrane indicates the presence of Fe_3O_4-NPs diffraction angles of 29.92°, 35.35°, 42.99°, 57.07°, and 62.58°. According to Match software analysis, Fe_3O_4-NPs data indicate structure 2101535 from the Crystallography Open Database [35] and related to the crystalline plane of [202], [311], [400], [333], and [404], respectively (Fig. 2). The peaks within the 2θ range of 10°–75° exhibited minimal variation, but the intensity of the peaks increased as the content of Fe_3O_4-NPs rose. The presence of Fe_3O_4-NPs within the BCA membrane was relatively weak, likely due to their growth on the surface of BCA membrane, which hindered the collecting of the diffraction peak data during the XRD test. However, higher Fe_3O_4-NPs content led to more self-agglomerated nanoparticles, resulting in a more real crystalline character. The peak intensity of the XRD pattern reflects the concentration of each element material. In the low content of Fe_3O_4-NPs, small peak intensities were observed that are associated with the low number of nanoparticles embedded homogeneously in the amorphous polymeric matrix [36]. The presence of more peaks in the BCA/Fe_3O_4-NPs 0.75 wt.% sample compared to the BCA/Fe_3O_4-NPs 1.0 wt.% sample is likely due to better dispersion and less agglomeration of nanoparticles at the lower concentration. At higher concentrations, agglomeration can cause a loss of long-range order, making it harder to detect distinct peaks, so it can reduce the number of distinct peaks due to overlapping signals and larger clusters of nanoparticles that change the particle orientation distribution [37]. Additionally, factors such as the interaction with the BCA matrix play important roles in diminishing the intensity of the XRD peaks.

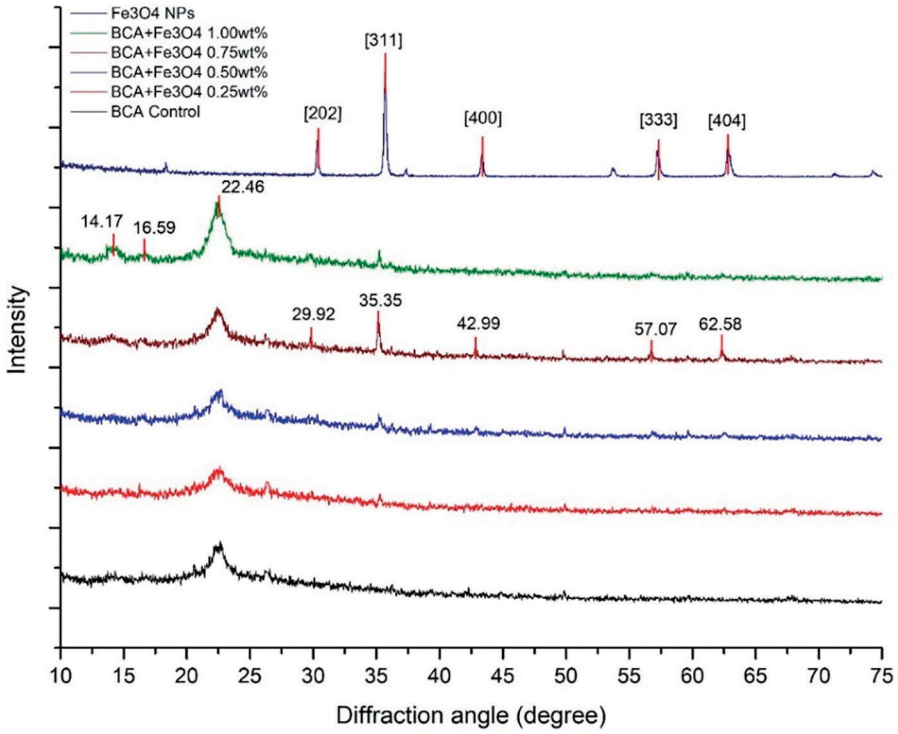

Figure 2: Diffractogram of BCA/Fe_3O_4-NPs membrane

Table 1: Structure analysis of BCA/Fe_3O_4-NPs membrane

Samples	d-spacings (nm)		Intensity (a.u.)		Crystallinity	
	d_{14}	d_{16}	I_{22}	I_{18}	CrI (%)	L (nm)
Control	0.618	0.534	152.66	69.71	54.34	14.19
BCA/Fe_3O_4-NPs 0.25 wt.%	0.617	0.527	120.27	61.13	49.17	16.39
BCA/Fe_3O_4-NPs 0.50 wt.%	0.615	0.534	127.79	62.49	51.10	19.45
BCA/Fe_3O_4-NPs 0.75 wt.%	0.619	0.543	139.46	56.65	59.38	19.70
BCA/Fe_3O_4-NPs 1.00 wt.%	0.624	0.534	198.46	62.86	68.33	20.11

The CrI of BCA membranes is 54.34% (Table 1). Adding Fe_3O_4-NPs of 0.25, 0.50, 0.75, and 1.00 wt.% into the membrane increases the CrI with values of 49.17%, 51.10%, 59.38%, and 68.33%, respectively. The crystallinity of nanocomposites can be further changed when nanoparticles are incorporated into cellulosic materials. Adding Fe_3O_4-NPs of 0.25 and 0.5 wt.% reduces the crystalline index of BCA membrane. Nanoparticles insert themselves between cellulose chains or interact with the hydroxyl groups on cellulose, arranging the cellulose network to become randomized cellulose and a subsequent reduction in crystalline value. This identic phenomenon of CrI reduction is reported in the rice husk fiber and sawdust after adding ferromagnetic nanoparticles [38,39] and bacterial cellulose membrane after being functionalized by copper nanoparticles [40] and hybrid of copper nanoparticle and graphene [18]. Interestingly, increasing the concentration of Fe_3O_4-NPs of 0.75 and 1.0 wt.% enhanced the CrI of the

BCA nanocomposite membrane. Higher content of Fe_3O_4-NPs interacts with the cellulose acetate matrix, enhancing the alignment of cellulose chains and inducing strong interfacial interactions, resulting in higher crystallinity. Roy et al. indicate that increasing nano-filler content enhances interfacial physical interactions between the polymer and nano-fillers, improving the orientation and crystallization of molecular chains [41].

The crystal size of BCA/Fe_3O_4-NPs membranes is 14.19, 16.39, 19.45, 19.70, and 20.11 nm in BCA membrane of control, Fe_3O_4-NPs content of 0.25, 0.50, 0.75 and 1.00 wt.%, respectively. Upon adding Fe_3O_4-NPs, an increase in crystallite size was evident, likely attributed to the integration of Fe_3O_4-NPs into BCA structure, given their inherently larger crystallite size (ranging from 9 to 53 nm) [42]. These findings collectively demonstrate that the inclusion of Fe_3O_4-NPs contributed to an overall enhancement in the crystalline nature of BCA membrane, which could have significant implications for the final properties of membrane.

3.3 Functional Group Analysis

Membrane samples were subjected to FTIR testing to examine the structural disparities pre and post-addition of nanomaterials. Fig. 3A shows the outcomes of these examinations. FTIR spectra of the BCA membrane were denoted by a black curve, and BCA membrane that was added with different concentrations of Fe_3O_4-NPs (0.25, 0.50, 0.75, and 1.00 wt.%) represented by the red, blue, green, and dark green curves, respectively. The wavenumber range was analyzed during the testing and scanned from 400 to 4000 cm^{-1}.

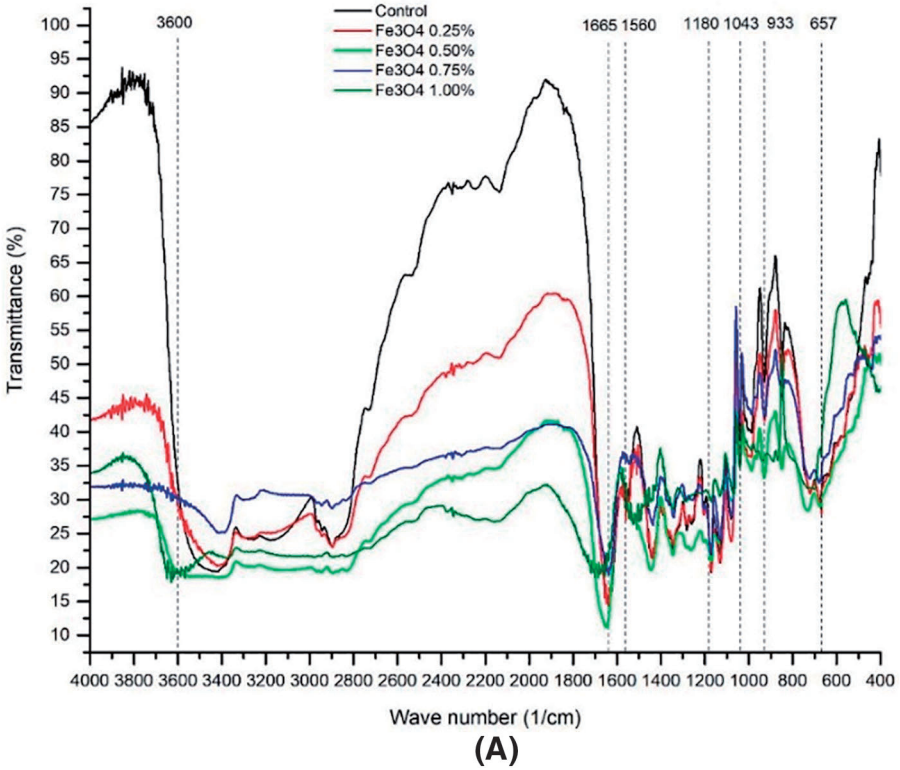

Figure 3: (Continued)

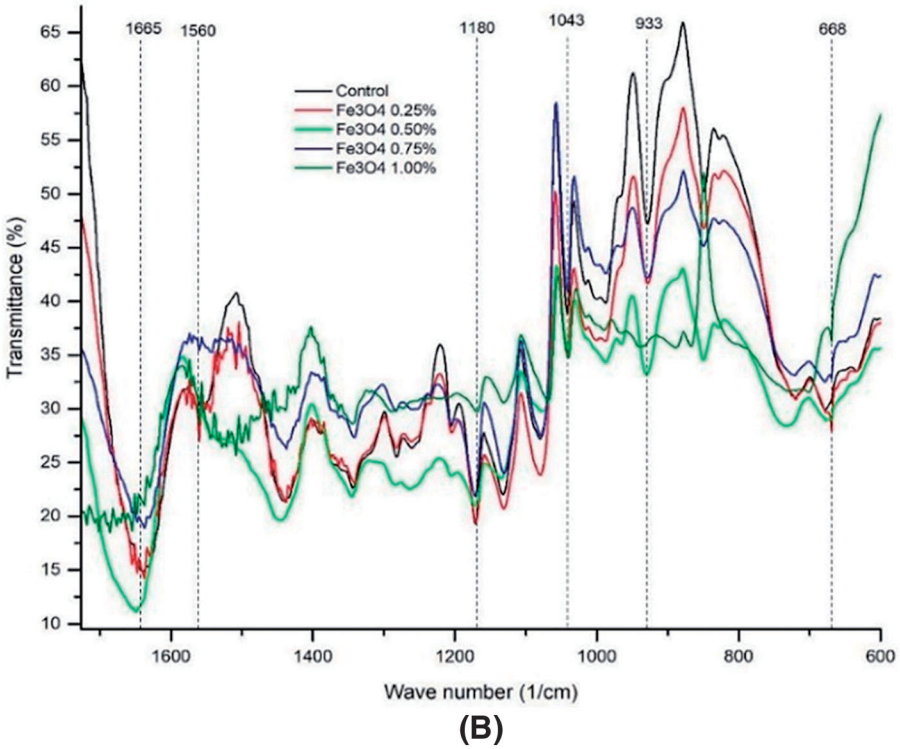

Figure 3: FTIR pattern: (A) Nanocomposite BCA membrane with Fe_3O_4-NPs content of 0.25, 0.50, 0.75 and 1.00 wt.%; (B) Deconvolution of FTIR pattern at wavenumber 1700–700 cm^{-1}

The presence of interaction of Fe_3O_4-NPs with BCA membrane is confirmed by the change in functional group peak in FTIR pattern. Some obvious changes were detected after comparing the Fe_3O_4-NPs added membrane and the original BCA membrane. Adding Fe_3O_4-NPs to the membrane causes a shifting of C-H stretching vibration in the 2700–3200 cm^{-1} range from the cellulose [43]. The broad peak observed in 3300–3600 cm^{-1} corresponds to OH-stretching, which is significant in determining hydrogen bonding. In regions of 760–1800 cm^{-1}, the spectrum of BCA/Fe_3O_4-NPs membrane exhibits modes typical for organic groups [44]. Deconvolution of the FTIR pattern (Fig. 3B) indicates that the transmittance of wavenumber 1665 cm^{-1} is reduced, which belongs to the C=O, representing the metal-oxygen vibration band [45]. The wavenumber of 1520–1400 cm^{-1} indicates the bending CH_2, C-H, and C-O groups in cellulose [46]. After adding Fe_3O_4-NPs by 0.75 wt.%, the peak at 1560 cm^{-1} is visible, indicating COO-Fe bond [47]. The region of 760–1180 cm^{-1} indicates the C-C stretching [44]. The peak at 1043 cm^{-1} is characteristic adsorption of β-glycosidic bond of cellulose [48] and the stretching vibration of C-O bonds can be recognized. The characteristic peaks presented at 933 cm^{-1} might be for the C-C out-of-plane deformations from cellulose acetate [49]. Peak presents a 657 cm^{-1} band related to Fe-O-C stretching vibration [50,51].

3.4 Magnetism Analysis

Various factors, such as crystallinity, size, shape, and crystal defects, significantly impact magnetic characteristics. To investigate the magnetic properties of our samples at room temperature, we employ a VSM device. Fig. 4 shows hysteresis loops in the nanocomposite membrane of BCA/Fe_3O_4-NPs. The control sample without Fe_3O_4-NPs has diamagnetic properties because it does not show a hysteresis curve. After adding Fe_3O_4-NPs into BCA, the membrane indicates the small hysteresis curve of magnetic materials.

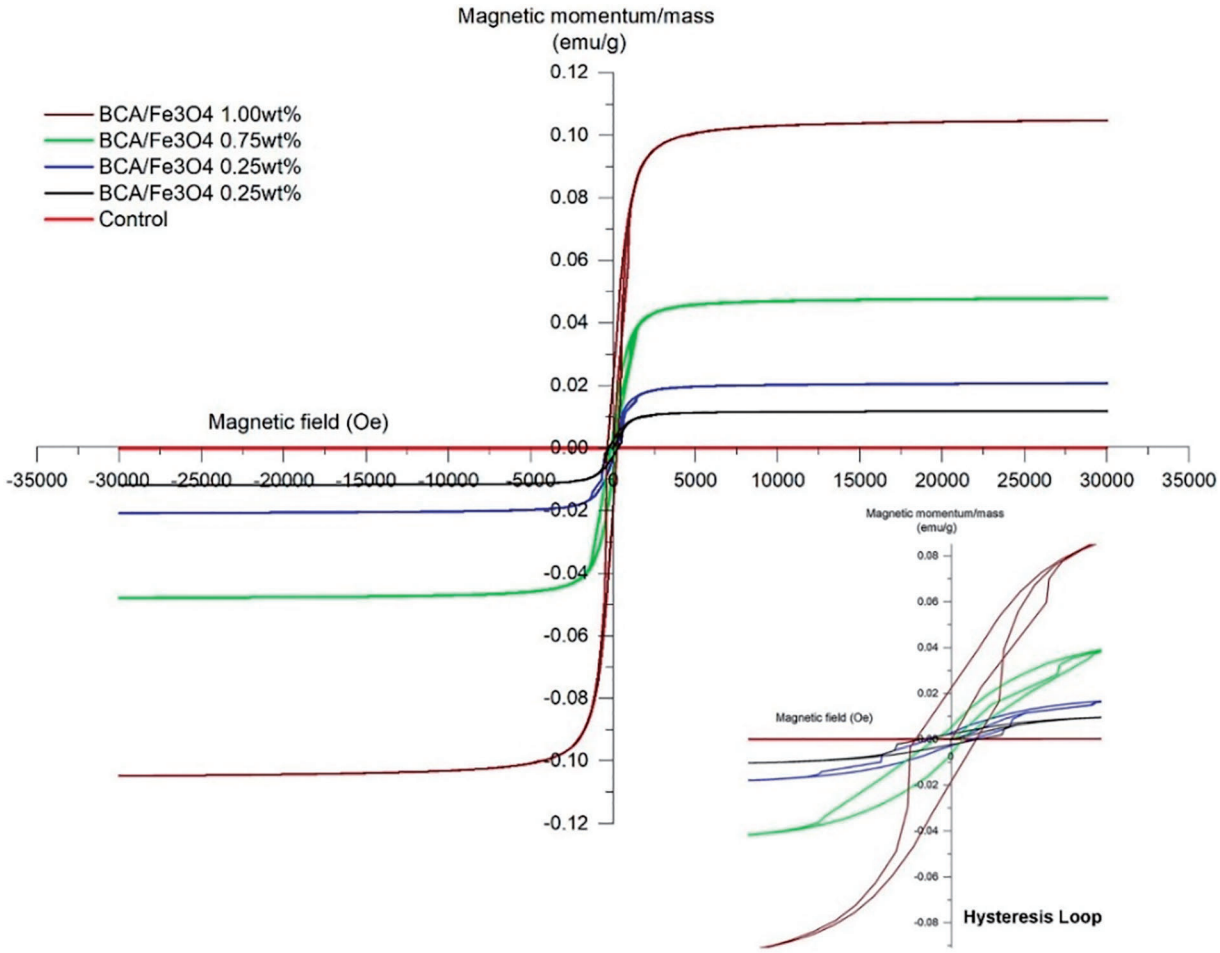

Figure 4: VSM curve of membrane BCA/Fe_3O_4-NPs

Table 2 shows the coercivity value (Hc) of the nanocomposite membrane, indicating a small value ranging from 200.01–333.18 Oe. After the addition of Fe_3O_4-NPs, the nature of the membrane nanocomposite changed from diamagnetic to paramagnetic. Higher content of Fe_3O_4-NPs results in higher magnetization saturation (Ms) and remanence (Mr). BCA/Fe_3O_4-NPs with Fe_3O_4-NPs content of 0.25, 0.50, 0.75, and 1 wt.% have Ms of 0.012, 0.021, 0.048, and 0.105 emu/g at 30 kOe, and Mr of 0.0025, 0.003, 0.006, and 0.023 emu/g, respectively (Table 2). Higher Ms can have a higher magnetic induction in its vicinity. Because Mr of Fe_3O_4 is 8.233 emu/g [52], Mr of the membrane increases inline Fe_3O_4-NPs content. Besides, increasing Mr is correlated with increasing particle size [53], as proved by Fig. 1, with higher agglomeration and crystal size increase from 14.19 to 20.22 nm (Table 1). It indicates that Fe_3O_4-NPs increase permanent magnetic properties and make the membrane more sensitive to the influence of magnetic field changes. It is beneficial in magnetic separation because it ensures that the magnetic particles or components being separated are fully magnetized and readily attracted to the magnetic field, enhancing the separation efficiency.

3.5 Antibacterial Properties

The antibacterial properties of BCA/Fe_3O_4-NPs membrane were tested using the disc-diffusion procedure against *S. aureus* and *E. coli*. In this procedure, the test disk was placed on the surface of inoculated test medium, and the wet disks absorbed water from the agar medium, initiating the release of

antimicrobial agents into the adjacent agar medium. Bacterial inhibition for control samples exhibits blur zones with diameter zones of 11.7 and 10.5 mm for *E. coli* and *S. aureus*, respectively (Fig. 5(AI)). Adding Fe_3O_4-NPs into BCA membrane increases zone inhibition size, and Fe_3O_4-NPs concentration of 0.25, 0.50, 0.75, and 1.0 wt.% exhibits a clear halo at inhibition with a measured diameter of 11.9, 12.2, 12.5, and 16.1 mm for *E. coli* and 10.4, 10,5, 10,5, 9.7, and 12.5 mm for *S. aureus*, respectively. It is clear that BCA/Fe_3O_4-NPs nanocomposite membranes have an antibacterial effect better against gram-negative bacteria (*E.coli*) compared to gram-positive bacteria (*S. aureus*).

Table 2: Magnetic properties of the membrane of BCA/Fe_3O_4-NPs

Samples	Ms (emu/g)	Mr (emu/g)	Hc (Oe)
Control	0.00	0.00	0.00
BCA/Fe_3O_4-NPs 0.25 wt.%	0.012	0.0025	249.55
BCA/Fe_3O_4-NPs 0.50 wt.%	0.021	0.003	215.55
BCA/Fe_3O_4-NPs 0.75 wt.%	0.048	0.006	200.01
BCA/Fe_3O_4-NPs 1.00 wt.%	0.105	0.023	333.18

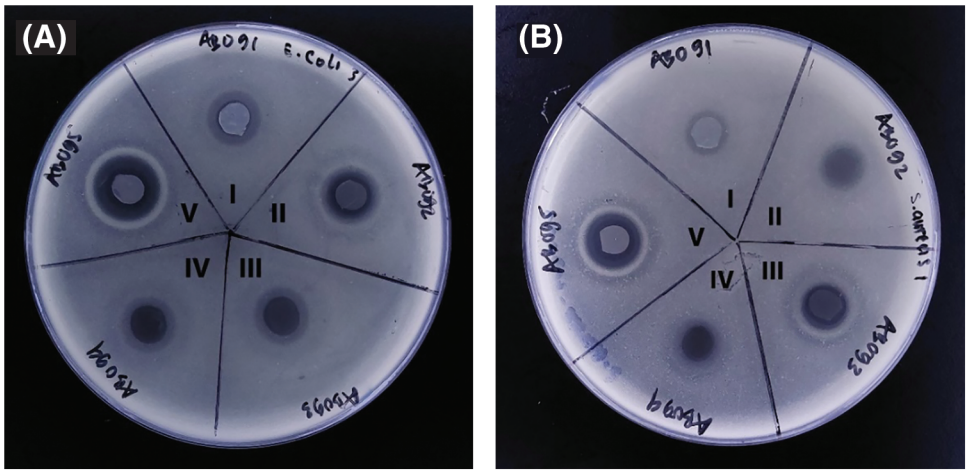

Figure 5: Antibacterial profile of nanocomposite BCA membrane (I) with Fe_3O_4-NPs 0.25 wt.% (II), 0.50 wt.% (III), 0.75 wt.% (IV), and 1 wt.% (V) using (A) *E .coli* and (B) *S. aureus*

One potential explanation for this antibacterial activity of the membrane is an attraction between the microbes that possess negative charges and nanoparticles with positive charges. While this attraction occurs, the microbes undergo rapid oxidation, leading to their immediate death. Typically, nanomaterials release ions that interact with thiol groups on the surface of bacterial cell proteins. This interaction causes the bacterial cells to break down [54]. Another mechanism that potentially triggered the antibacterial effect of the particles is reactive oxygen species (ROS), causing induction of oxidative stress in bacteria [55,56]. The ROS is generated by the iron oxide [57], which could have suppressed various bacteria, including *S. aureus* and *E. coli*. ROS encompasses radicals such as hydroxyl radicals (-OH), superoxide radicals (O_2^-), hydrogen peroxide (H_2O_2), and it's plausible that singlet oxygen ($^1O_2$) contributed to resulting in damage or genomic instability within the bacterial cells [58].

3.6 Dye Adsorption

The BCA composite membrane capability to adsorb the dye, including anionic and cationic dye, in water has also been measured. Fig. 6 shows the absorbance of nanocomposite BCA membranes after absorbing MB, CR, AO, and Rh dye. The dye adsorption of nanocomposite BCA membranes is shown in Table 3. BCA nanocomposite membrane adsorbs MB and Rh at the lowest value of 12.3 and 0.21 mgL^{-1} at Fe_3O_4-NPs concentration of 0.75 and 1.0 wt.% or reduced by 49.1% and 82.2%, respectively, when compared to adsorption of the control. Adsorption of MB in BCA with Fe_3O_4-NPs 1.0 wt.% less than BCA with Fe_3O_4-NPs 0.5 wt.% due to agglomeration of NPs. Nano-scaled particles possess high surface energy due to large proportion of surface atoms. To minimize this energy, they naturally tend to stick together. This tendency to agglomerate in Fe_3O_4-NPs increases by the magnetic dipole-dipole attractions between them [59]. A higher content of Fe_3O_4-NPs tends to agglomerate, and agglomeration reduces the effective surface area of nanoparticles that are available for interaction with Methylene Blue, thus decreasing the adsorption capacity. This phenomenon is the opposite of anionic dyes, such as CR and AO. BCA nanocomposite membrane adsorbs CR and AO at the highest value of 8.95 and 4.44 mgL^{-1} at Fe_3O_4-NPs concentration of 0.25 and 0.75 wt.% or increased by 56.5% and 107.5%, respectively.

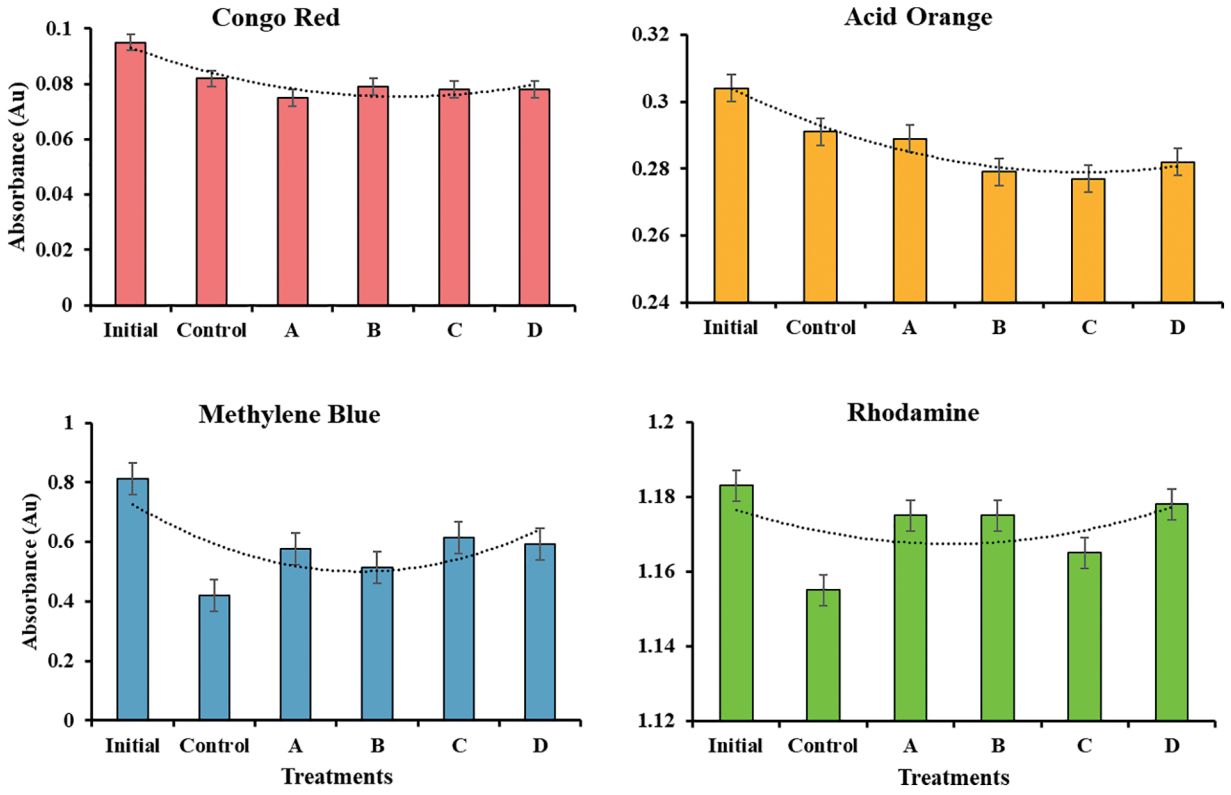

Figure 6: The absorbance of nanocomposite BCA membrane for CR, AO, MB, and Rh dyes (Treatment (A) BCA/Fe_3O_4-NPs 0.25 wt.%; (B) BCA/Fe_3O_4-NPs 0.50 wt.%; (C) BCA/Fe_3O_4-NPs 0.75 wt.%; (D) BCA/Fe_3O_4-NPs 1.00 wt.%)

MB and Rh are easier to be removed from the water because they are cationic dyes (positive charge), so they have more intermolecular interaction with hydroxyl groups (-OH) at the whole cellulose molecule [60,61]. Many metal oxide nanoparticles (e.g., Fe_3O_4) naturally have hydroxyl groups on their surfaces due to dissociative chemisorption of water on the magnetite surfaces [62]. These interactions of

Fe_3O_4-NPs provide more hydroxyl groups in the membrane and allow cellulose to absorb the dye effectively. Fe_3O_4-NPs have a positive charge in a neutral aqueous solution [63] so they reduce the adsorption of cationic dye because of reduced hydrophilic properties of the BCA membrane after interaction with Fe_3O_4-NPs. The positive charge of Fe_3O_4-NPs in a neutral aqueous solution causes them to easily interact with anionic dyes like CR and AO. Anionic dyes have a repulsion to the hydroxyl group in cellulose, so CR and AO adsorption increases after adding Fe_3O_4-NPs into BCA membrane.

Table 3: Dye adsorption by BCA nanocomposite membrane

Sample	Adsorption of dyes (mgL^{-1})			
	MB	Rh	CR	AO
Control	48.3% (24.17)	2.4% (1.18)	13.7% (6.84)	4.3% (2.14)
BCA/Fe_3O_4-NPs 0.25 wt.%	29.0% (14.51)	0.7% (0.34)	21.1% (10.53)	4.9% (2.47)
BCA/Fe_3O_4-NPs 0.50 wt.%	36.8% (18.39)	0.7% (0.34)	16.8% (8.42)	8.2% (4.11)
BCA/Fe_3O_4-NPs 0.75 wt.%	24.6% (12.30)	1.5% (0.76)	17.9% (8.95)	8.9% (4.44)
BCA/Fe_3O_4-NPs 1.00 wt.%	27.3% (13.65)	0.4% (0.21)	17.9% (8.95)	7.3% (3.62)

3.7 Bacteria Adhesion

The results of the bacteria adhesion test with the water samples taken from 2 rivers are shown in Fig. 7. The initial bacterial amount in River A was 7.95×10^{17} CFU/mL, and in River B was 2.1×10^{18} CFU/mL. After immersion, the percentage of bacteria remaining in the samples after immersion in the membrane ranged from 51.04%–65.8% in River A, and 39.1%–67.4% in River B. The initial number of bacteria in the sample influenced the percentage of bacterial residue. The greater the initial number of bacteria in the sample, the more the percentage of bacteria remaining after immersion in the same surface area of the nanofilter. This is caused by the adsorption capacity of the membrane used. The river water samples were objects that not only contained microorganisms but also domestic waste from housing, where the waste is composed of organic and inorganic materials. Thus, competition occurs in the process of binding these materials to the membrane surface, especially those that have been enriched with magnetite. Some bacteria strains, which are a group of gram-negative prokaryotes, have characteristics of magnetotactic bacteria, bacteria that contain magnetic nanoparticles along the chain configuration in their cells [64,65]. Although the structure of gram-negative and gram-positive bacteria is different, most of them have a negative charge [66], while Fe_3O_4-NPs have a positive charge in neutral and acidic aqueous solutions [63]. The bacteria interact and enable them to adhere to each other through magnetite attraction [67] and electrostatic interaction [68] between positively charged magnetic nanoparticles and negatively charged bacterial cells, so increasing magnetite content in the membrane causes an increase in bacteria adhesion.

3.8 Tensile Strength

The results of tensile test are depicted in Fig. 8. Tensile tests show that the membranes have tensile strength of 38.79 ± 2.94, 39.26 ± 4.0, 64.94 ± 11.22, 67.09 ± 4.68, and 38.08 ± 4.41 MPa, for membranes with content of Fe_3O_4-NPs of 0.25, 0.50, 0.75, and 1.0 wt.%, respectively. Fe_3O_4-NPs influence the tensile strength of BCA membrane significantly after statistical analysis conducted using one-way ANOVA (significant level of 0.05, n = 5, p value = 0.000). Tukey test indicates that adding Fe_3O_4-NPs of 0.50 and 0.75 wt.% into BCA membrane results differently in tensile test compared to control.

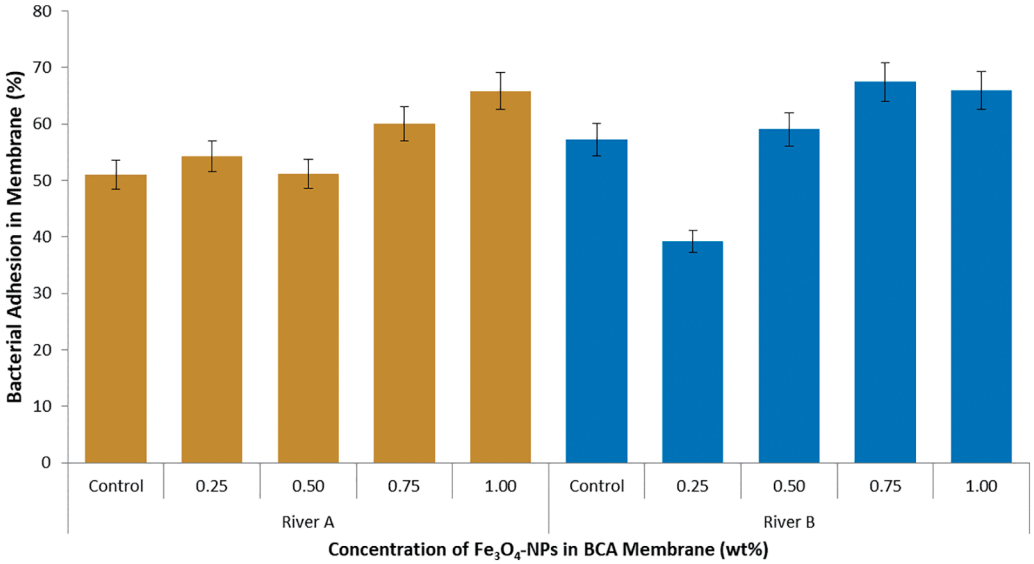

Figure 7: Bacteria adhesion in BCA membrane after immersed in wastewater of River A and River B

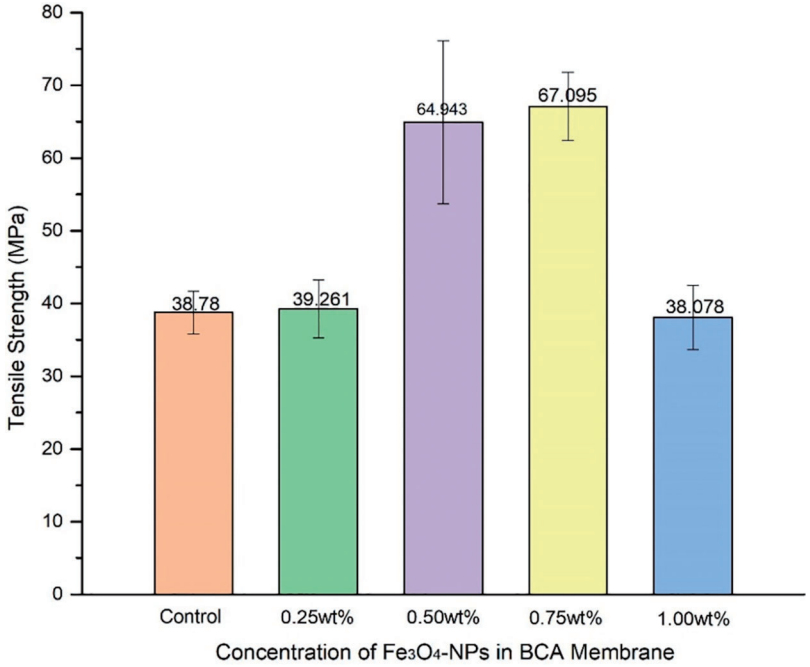

Figure 8: Tensile strength of BCA nanocomposite membrane with various Fe_3O_4-NPs content

The strong interaction has occurred through chemical interaction of the hydroxyl groups of BCA with Fe_3O_4-NPs [69] BCA nanocomposite. The highest content of Fe_3O_4-NPs reduces the tensile strength of BCA nanocomposite because of a high agglomeration of Fe_3O_4-NPs. Fe_3O_4-NPs tend to agglomerate so they cannot integrate into BCA network because they remain outside the membrane network and do not bind effectively to cellulose. As a result, they do not enhance the mechanical properties and actually reduce the membrane strength. This was confirmed by tensile test results, which showed that the strength of BCA membrane with Fe_3O_4-NPs of 1.0 wt.% is lower than Fe_3O_4-NPs content of 0.75 wt.%. It is

fathomed that Fe_3O_4-NPs agglomeration may occur which leads to the reduction of tensile strength. Agglomeration reduces the effective surface area of nanoparticles to interact chemically with hydroxyl groups of BCA. Lower interaction means less chemical bonding present, resulting in less strength of the membrane. This was supported by the previous studies that high content of Fe_3O_4-NPs decreases its strength of cellulose membrane [70,71].

4 Conclusions

The exploration of the utilization of pineapple biowaste extract to produce BCA membranes functionalized with Fe_3O_4-NPs and revealed their membrane characteristics were successfully investigated. Observations of membrane surface indicate a tendency for Fe_3O_4-NPs to form clusters. The interplay between BCA and Fe_3O_4-NPs within the nanocomposite system was illustrated by a new peak emerging at around 1530 cm^{-1} and a shifting band at 1665 cm^{-1}. Moreover, the alterations in membrane crystallinity attributes were evident through an enhanced crystallinity index. Adding Fe_3O_4-NPs into the BCA membrane causes magnetic properties to change from non-magnetic membrane to paramagnetic membrane properties. They also increase the antibacterial inhibition against *E. coli* and *S. aureus*, enhance the adsorption of anionic dye type, and increase bacterial adhesion into the membrane so the membrane can adsorb bacteria from wastewater from rivers ranging from 39.1% to 67.4%. Adding Fe_3O_4-NPs into the BCA nanocomposite membrane with concentration of 0.75 wt.% results in the highest tensile strength of 67.09 ± 4.68 MPa or increase of 37% compared to BCA membrane. Hence, these findings can be developed as the filtration membrane for wastewater treatment. However, in the future, the challenge includes exploring methods to get more homogenized nanoparticles in the membrane and applying this membrane to specific equipment for a practical approach.

Acknowledgement: The authors express their sincere thanks to LPPM Universitas Negeri Malang, which has funded this research under the scheme Riset Kolaborasi Indonesia.

Funding Statement: This study was funded by LPPM Universitas Negeri Malang with Contract No. 10.5.31/UN32.20.1/LT/2023.

Author Contributions: All authors have contributed to this study, including conceptual design, material preparation, experiment, data analysis, and writing the manuscript. Heru Suryanto, as a granted receiver, conducted the preparation of materials, data analysis and wrote the main manuscript. Daimon Syukri and Uun Yanuhar contributed to data collection and prepared Figs. 6 and 7. Fredy Kurniawan and Sahrul Efendi prepared a magnetic analysis. Jibril Maulana and Komarudin Komarudin contributed to synthesizing the membrane acetate. Nico Rahman Caesar and Fajar Nusantara contributed to antibacterial and structure analysis. Joseph Selvi Binoj has done a finishing in data analysis and writing the manuscript. All authors reviewed the results and approved the final version of the manuscript.

Availability of Data and Materials: Not applicable.

Ethics Approval: Not applicable.

Conflicts of Interest: The authors declare that they have no conflicts of interest to report regarding the present study.

References

1. Mujtaba M, Fernandes FL, Fazeli M, Mukherjee S, Savassa SM, de Medeiros AG, et al. Lignocellulosic biomass from agricultural waste to the circular economy: a review with focus on biofuels, biocomposites and bioplastics. J Clean Prod. 2023;402:136815. doi:10.1016/j.jclepro.2023.136815.
2. OEC. Cellulose. Available from: https://oec.world/en/profile/hs/cellulose. [Accessed 2024].

3. Chatterjee S, Sharma S, Prasad RK, Datta S, Dubey D, Meghvansi MK, et al. Cellulase enzyme based biodegradation of cellulosic materials: an overview. South Asian J Exp Biol. 2016;5(6):271–82. doi:10.38150/sajeb.5(6).p271-282.
4. Rizaty MA. Pineapple becomes the leading fruit commodity with the highest export volume. Available from: https://databoks.katadata.co.id/datapublish/2021/03/12/nanas-jadi-komoditas-buah-unggulan-dengan-volume-ekspor-tertinggi. [Accessed 2021].
5. Saraswaty V, Risdian C, Primadona I, Andriyani R, Andayani DGS, Mozef T. Pineapple peel wastes as a potential source of antioxidant compounds. IOP Conf Ser Earth Environ Sci. 2017;60:012013. doi:10.1088/1755-1315/60/1/012013.
6. Lupaşcu RE, Ghica MV, Dinu-Pîrvu CE, Popa L, Velescu BŞ, Arsene AL. An overview regarding microbial aspects of production and applications of bacterial cellulose. Materials. 2022;15:1–14. doi:10.3390/ma15020676.
7. Kim D-Y, Nishiyama Y, Kuga S. Surface acetylation of bacterial cellulose. Cellulose. 2002;9:361–67. doi:10.1023/A:1021140726936.
8. Su Z, Liu T, Li X, Graham N, Yu W. Beneficial impacts of natural biopolymers during surface water purification by membrane nanofiltration. Water Res. 2021;201:117330. doi:10.1016/j.watres.2021.117330.
9. Jaleh B, Nasrollahzadeh M, Nasri A, Eslamipanah M, Moradi A, Nezafat Z. Biopolymer-derived (nano)catalysts for hydrogen evolution *via* hydrolysis of hydrides and electrochemical and photocatalytic techniques: a review. Int J Biol Macromol. 2021;182:1056–90. doi:10.1016/j.ijbiomac.2021.04.087.
10. Musa MT, Shaari N, Kamarudin SK, Wong WY. Recent biopolymers used for membrane fuel cells: characterization analysis perspectives. Int J Energy Res. 2022;46:16178–207. doi:10.1002/er.8329.
11. Jabbari F, Babaeipour V. Bacterial cellulose as a potential biopolymer for wound care. A review. Int J Polym Mater. 2024;73:455–77. doi:10.1080/00914037.2023.2167080.
12. Islam MdD, Uddin FJ, Rashid TU, Shahruzzaman M. Cellulose acetate-based membrane for wastewater treatment—a state-of-the-art review. Mater Adv. 2023;4:4054–102. doi:10.1039/D3MA00255A.
13. Ghaseminezhad SM, Barikani M, Salehirad M. Development of graphene oxide-cellulose acetate nanocomposite reverse osmosis membrane for seawater desalination. Compos B Eng. 2019;161:320–7. doi:10.1016/j.compositesb.2018.10.079.
14. El-Din LAN, El-Gendi A, Ismail N, Abed KA, Ahmed AI. Evaluation of cellulose acetate membrane with carbon nanotubes additives. J Ind Eng Chem. 2015;26:259–64. doi:10.1016/j.jiec.2014.11.037.
15. Jain H, Verma AK, Dhupper R, Wadhwa S, Garg MC. Development of CA-TiO_2-incorporated thin-film nanocomposite forward osmosis membrane for enhanced water flux and salt rejection. Int J Environ Sci Technol. 2022;19:5387–00. doi:10.1007/s13762-021-03415-x.
16. Rakhshan N, Pakizeh M. The effect of functionalized SiO_2 nanoparticles on the morphology and triazines separation properties of cellulose acetate membranes. J Ind Eng Chem. 2016;34:51–60. doi:10.1016/j.jiec.2015.10.031.
17. El-Noss M, Isawi H, Shawky HA, Gomaa MA, Abdel-Mottaleb MSA. Improvement of cellulose acetate forward osmosis membrane performance using zinc oxide nanoparticles. Desalin Water Treat. 2020;193:19–33. doi:10.5004/dwt.2020.25677.
18. Suryanto H, Susilo BD, Maulana J, Aminnudin, Yanuhar U, Wonorahardjo S, et al. Characterization of nanocomposite membrane based bacterial cellulose made of pineapple waste reinforced by graphite nanoplatelets. J Renew Mater. 2022;10(9):2455–65. doi:10.32604/jrm.2022.020478.
19. Maulana J, Suryanto H, Aminnudin A. Effect of graphene addition on bacterial cellulose-based nanocomposite. J Mechanical Eng Sci Technol. 2022;6(2):107–12. doi:10.17977/um016v6i22022p107.
20. Zhang Z, Li H, Sui H, He L, Li X. Synthesis and application of hydrophilically-modified Fe_3O_4 nanoparticles in oil sands separation. RSC Adv. 2018;8(28):15813–24. doi:10.1039/C8RA01966E.
21. Yingkamhaeng N, Intapan I, Sukyai P. Fabrication and characterisation of functionalised superparamagnetic bacterial nanocellulose using ultrasonic-assisted *in situ* Synthesis. Fibers Polym. 2018;19(3):489–97. doi:10.1007/s12221-018-7738-6.

22. Talbot D, Queiros Campos J, Checa-Fernandez BL, Marins JA, Lomenech C, Hurel C, et al. Adsorption of organic dyes on magnetic iron oxide nanoparticles. Part I: mechanisms and adsorption-induced nanoparticle agglomeration. ACS Omega. 2021;6(29):19086–98. doi:10.1021/acsomega.1c02401.
23. Elsacker E, Vandelook S, Damsin B, Van Wylick A, Peeters E, De Laet L. Mechanical characteristics of bacterial cellulose-reinforced mycelium composite materials. Fungal Biol Biotechnol. 2021;8(1):1–14. doi:10.1186/s40694-021-00125-4.
24. Yu K, Spiesz EM, Balasubramanian S, Schmieden DT, Meyer AS, Aubin-Tam ME. Scalable bacterial production of moldable and recyclable biomineralized cellulose with tunable mechanical properties. Cell Rep Phys Sci. 2021;2(6):100464. doi:10.1016/j.xcrp.2021.100464.
25. Baig MMFA, Fatima A, Gao X, Farid A, Khan MA, Zia AW, et al. Disrupting biofilm and eradicating bacteria by Ag-Fe_3O_4@MoS_2 MNPs nanocomposite carrying enzyme and antibiotics. J Controlled Release. 2022;352:98–120. doi:10.1016/j.jconrel.2022.10.009.
26. Yanuhar U, Suryanto H, Sardjono SA, Ningrum IK, Aminnudin A, Binoj JS. Effect of titanium dioxide nanoparticle on properties of nanocomposite membrane made of bacterial cellulose. J Nat Fibers. 2022;19(16):13914–27. doi:10.1080/15440478.2022.2112797.
27. Suryanto H, Muhajir M, Susilo BD, Pradana YRA, Wijaya HW, Saad Ansari A, et al. Nanofibrillation of bacterial cellulose using high-pressure homogenization and its films characteristics. J Renew Mater. 2021;9(10):1717–28. doi:10.32604/jrm.2021.015312.
28. Suryanto H, Kurniawan F, Syukri D, Binoj JS, Hari PD, Yanuhar U. Properties of bacterial cellulose acetate nanocomposite with TiO_2 nanoparticle and graphene reinforcement. Int J Biol Macromol. 2023;235:123705. doi:10.1016/j.ijbiomac.2023.123705.
29. Cobo FN, Faria-Tisher PCS, Duarte JL, Carvalho GM. Preparation and characterization of microporous cellulose acetate films using breath figure method by spin coating technique. Cellulose. 2017;24(11):4981–95. doi:10.1007/s10570-017-1459-7.
30. Segal L, Creely JJ, Martin AE, Conrad CM. An empirical method for estimating the degree of crystallinity of native cellulose using the X-ray diffractometer. Text Res J. 1959;29(10):786–94. doi:10.1177/00405175590 2901003.
31. Balouiri M, Sadiki M, Ibnsouda SK. Methods for *in vitro* evaluating antimicrobial activity: a review. J Pharm Anal. 2016;6(2):71–9. doi:10.1016/j.jpha.2015.11.005.
32. Herbert RA. Methods for enumerating microorganisms and determining biomass in natural environments. In: Grigorova R, Norris JR, editors. Techniques in microbial ecology. USA: Academic Press; 1990. p. 1–39. doi:10.1016/S0580-9517(08)70238-1.
33. Haruna MA, Wen D. Surface functionalized Fe_3O_4-polyacrylamide dispersion for improved oil recovery at harsh conditions. J Appl Polym Sci. 2023;140(36):e54383. doi:10.1002/app.54383.
34. Wada M, Okano T, Sugiyama J. Allomorphs of native crystalline cellulose I evaluated by two equatorial d-spacings. J Wood Sci. 2001;47:124–8. doi:10.1007/BF00780560.
35. Okudera H, Kihara K, Matsumoto T. Temperature dependence of structure parameters in natural magnetite: single crystal X-ray studies from 126 to 773 K. Acta Crystallogr B. 1996;52(3):450–7. doi:10.1107/S0108768196 000845.
36. Garcia AM, Martins TS, Camilo FF. Free facile preparation of Ag-nanoparticles on cellulose membrane for catalysis. Cellulose. 2021;28(8):4899–911. doi:10.1007/s10570-021-03827-5.
37. Binns J, Darmanin C, Kewish CM, Pathirannahalge SK, Berntsen P, Adams PLR, et al. Preferred orientation and its effects on intensity-correlation measurements. IUCrJ. 2022 Mar 1;9:231–42. doi:10.1107/S2052252521012422.
38. Effendi EZ, Hariady YC, Salaahuddin MD, Irawan C, Nata IF. Utilization of rice husk cellulose as a magnetic nanoparticle biocomposite fiber source for the absorption of manganese (Mn^{2+}) ions in peat water. J Kimia Sains dan Aplikasi. 2019;22(6):220–6. doi:10.14710/jksa.22.6.220-226.
39. Suryanto H, Yanuhar U, Puspitasari P, Aminnudin, Yanuhar U, Maulana J, et al. Morphology and structure of sawdust waste after adding magnetic nanoparticles. E3S Web Conf. 2024;473:03001. doi:10.1051/e3sconf/202447303001.

40. Yanuhar U, Suryanto H, Amin M, Binoj JS, Casuarina I. Green synthesis of nano-copper oxide using Sargassum sp. functionalized in cellulose acetate membrane for dye adsorption. Glob J Environ Sci Manag. 2024;10(4):1933–50. doi:10.22034/gjesm.2024.04.26.
41. Roy A, Panda S, Gupta J, Anu, Singh RP, Deeksha, et al. Effects of interfacial interactions on structural, optical, thermal degradation properties and photocatalytic activity of low-density polyethylene/$BaTiO_3$ nanocomposite. Polymer. 2023;276:125932. doi:10.1016/j.polymer.2023.125932.
42. Upadhyay S, Parekh K, Pandey B. Influence of crystallite size on the magnetic properties of Fe_3O_4 nanoparticles. J Alloys Compd. 2016;678:478–85. doi:10.1016/j.jallcom.2016.03.279.
43. Zhbankov RG. Methods for obtaining the infrared spectra of cellulose and related materials. In: Zhbankov RG, editor. Infrared spectra of cellulose and its derivatives. Boston: Springer; 1966. p. 1–33. doi: 10.1007/978-1-4899-2732-3_1.
44. Lesiak B, Rangam N, Jiricek P, Gordeev I, Tóth J, Kövér L, et al. Surface study of Fe_3O_4 nanoparticles functionalized with biocompatible adsorbed molecules. Front Chem. 2019;7(642):1–16. doi:10.3389/fchem.2019.00642.
45. Sivasankari S, Kalaivizhi R, Gowriboy N. Cellulose acetate (CA) membrane tailored with Fe_3O_4@ZnO core shell nanoparticles: fabrication, structural analysis and its adsorption analysis. ChemistrySelect. 2021;6(9):2350–9. doi:10.1002/slct.202004689.
46. Suciyati SW, Manurung P, Sembiring S, Situmeang R. Comparative study of *Cladophora* sp. cellulose by using FTIR and XRD. J Phys Conf Ser. 2021;1751(1):012075. doi:10.1088/1742-6596/1751/1/012075.
47. Calvini P, Silveira M. FTIR analysis of naturally aged $FeCl_3$ and $CuCl_2$-doped cellulose papers. E-Preserv Sci. 2008;5:1–6.
48. Trisnawati L, Helmiyati H. Cellulose-Fe_3O_4 nanocomposite based on rice husk as catalyst for synthesis of methyl ester from waste cooking oil. IOP Conf Ser Mater Sci Eng. 2020;763(1):012012. doi:10.1088/1757-899X/763/1/012012.
49. Goda ES, Nour MA, Hong SE, Lee S, Bin, Kim IS, et al. Facile route for the decoration of nickel hydroxide sheets as antibacterial nanocomposite for cellulose acetate butyrate films. Egypt J Chem. 2022;65(1):501–10. doi:10.21608/ejchem.2021.79268.4046.
50. Zanata L, Tofanello A, Martinho HS, Souza JA, Rosa DS. Iron oxide nanoparticles-cellulose: a comprehensive insight on nanoclusters formation. J Mater Sci. 2022;57(1):324–35. doi:10.1007/s10853-021-06564-z.
51. Lee KE, Morad N, Teng TT, Poh BT. Development, characterization and the application of hybrid materials in coagulation/flocculation of wastewater: a review. Chem Eng J. 2012;203:370–86. doi:10.1016/j.cej.2012.06.109.
52. Sayoga IMA, Sujita S. Characterization of magnetic properties of ferric oxide from Sekotong beach iron sand West Lombok Indonesia. World J Adv Eng Eng Technol Sci. 2022;5(2):82–7. doi:10.30574/wjaets.2022.5.2.0051.
53. Li Q, Kartikowati CW, Horie S, Ogi T, Iwaki T, Okuyama K. Correlation between particle size/domain structure and magnetic properties of highly crystalline Fe_3O_4 nanoparticles. Sci Rep. 2017;7(1):9894. doi:10.1038/s41598-017-09897-5.
54. Prabhu YT, Rao KV, Kumari BS, Kumar VSS, Pavani T. Synthesis of Fe_3O_4 nanoparticles and its antibacterial application. Int Nano Lett. 2015;5(2):85–92. doi:10.1007/s40089-015-0141-z.
55. Vaishampayan A, Grohmann E. Antimicrobials functioning through ROS-mediated mechanisms: current insights. Microorganisms. 2022;10(1):1–10. doi:10.3390/microorganisms10010061.
56. Van Acker H, Coenye T. The role of reactive oxygen species in antibiotic-mediated killing of bacteria. Trends Microbiol. 2017;25(6):456–66. doi:10.1016/j.tim.2016.12.008.
57. Kessler A, Hedberg J, Blomberg E, Odnevall I. Reactive oxygen species formed by metal and metal oxide nanoparticles in physiological media: a review of reactions of importance to nanotoxicity and proposal for categorization. Nanomaterials. 2022;12(11):1–24. doi:10.3390/nano12111922.
58. Schieber M, Chandel NS. ROS function in redox signaling and oxidative stress. Curr Biol. 2014;24(10):1–25. doi:10.1016/j.cub.2014.03.034.

59. Yeap SP, Lim J, Ooi BS, Ahmad AL. Agglomeration, colloidal stability, and magnetic separation of magnetic nanoparticles: collective influences on environmental engineering applications. J Nanoparticle Res. 2017;19(11):368. doi:10.1007/s11051-017-4065-6.
60. Oh JE, Park N-M. Hydrophilic, transparent, and stretchable film using unmodified cellulose fibers. Mater Lett. 2022;309:131385. doi:10.1016/j.matlet.2021.131385.
61. Akter M, Bhattacharjee M, Dhar AK, Rahman FBA, Haque S, Rashid TU, et al. Cellulose-based hydrogels for wastewater treatment: a concise review. Gels. 2021;7(1). doi:10.3390/gels7010030.
62. Kendelewicz T, Liu P, Doyle CS, Brown GE, Nelson EJ, Chambers SA. Reaction of water with the (100) and (111) surfaces of Fe_3O_4. Surf Sci. 2000;453(1):32–46. doi:10.1016/S0039-6028(00)00305-8.
63. Yu H, Li Y, Li X, Fan L, Yang S. Highly dispersible and charge-tunable magnetic Fe_3O_4 nanoparticles: facile fabrication and reversible binding to GO for efficient removal of dye pollutants. J Mater Chem A. 2014;2(38):15763–7. doi:10.1039/C4TA03476G.
64. Chariaou M, Rahn-Lee L, Kind J, García-Rubio I, Komeili A, Gehring AU. Anisotropy of bullet-shaped magnetite nanoparticles in the magnetotactic bacteria desulfovibrio magneticus sp. strain RS-1. Biophys J. 2015;108(5):1268–74. doi:10.1016/j.bpj.2015.01.007.
65. Wang X, Li Y, Zhao J, Yao H, Chu S, Song Z, et al. Magnetotactic bacteria: characteristics and environmental applications. Front Environ Sci Eng. 2020;14(4):1–14. doi:10.1007/s11783-020-1235-z.
66. Wilson WW, Wade MM, Holman SC, Champlin FR. Status of methods for assessing bacterial cell surface charge properties based on zeta potential measurements. J Microbiol Methods. 2001;43(3):153–64. doi:10.1016/S0167-7012(00)00224-4.
67. Nguyen MD, Tran HV, Xu S, Lee TR. Fe_3O_4 nanoparticles: structures, synthesis, magnetic properties, surface functionalization, and emerging applications. Appl Sci. 2021;11(23):1–34. doi:10.3390/app112311301.
68. Li Z, Ma J, Ruan J, Zhuang X. Using positively charged magnetic nanoparticles to capture bacteria at ultralow concentration. Nanoscale Res Lett. 2019;14(1):195. doi:10.1186/s11671-019-3005-z.
69. Zhu X, Zhang L, Zou G, Chen Q, Guo Y, Liang S, et al. Carboxylcellulose hydrogel confined-Fe_3O_4 nanoparticles catalyst for Fenton-like degradation of Rhodamine B. Int J Biol Macromol. 2021;180:792–803. doi:10.1016/j.ijbiomac.2021.04.067.
70. Kaco H, Baharin KW, Zakaria S, Chia CH, Jaafar SNS, Gan SY, et al. Preparation and characterization of Fe_3O_4/regenerated cellulose membrane. Sains Malays. 2017;46(4):623–8. doi:10.17576/jsm-2017-4604-15.
71. Khandanlou R, Ahmad MB, Shameli K, Saki E, Kalantari K. Studies on properties of rice straw/polymer nanocomposites based on polycaprolactone and Fe_3O_4 nanoparticles and evaluation of antibacterial activity. Int J Mol Sci. 2014;15(10):18466–83. doi:10.3390/ijms151018466.